

Image oversampling for page-oriented optical data storage

Mark Ayres, Alan Hoskins, and Kevin Curtis

Page-oriented data storage systems incorporate optical detector arrays [such as complementary metal-oxide semiconductor (CMOS) arrays] in order to read data images. For laboratory demonstrations the detector array is typically pixel matched to the data image [Opt. Lett. **22**, 1509 (1997)]. This approach requires exceedingly high-performance optics and mechanics for the simultaneous alignment of each data-bearing pixel image to a detector element to be achieved. Systems intended for commercialization are designed with detector arrays that spatially sample the image at or above the Nyquist rate in order to read poorly aligned and distorted images [S. Redfield, *Holographic Data Storage* (Springer-Verlag, 2000), pp. 347–349]. However, for data page sizes exceeding a megapixel this approach becomes prohibitive in terms of detector bandwidth, size, power, cost, and processing requirements. We have instead developed a sub-Nyquist oversampling methodology that can recover arbitrarily aligned and distorted megapixel data page images with pixel-matched fidelity by using fewer than double the number of detector pixels. Features required for practicable implementation are described, including fiducials for alignment determination. © 2006 Optical Society of America

OCIS codes: 210.2860, 210.4680.

1. Introduction

Holography has long held promise as a data storage technology with the potential for vast capacity and high data rates.¹ Recent advances in materials, multiplexing architectures, and components are finally making this vision a reality.² Among the final issues to be resolved are the engineering challenges of the systems that permit heretofore expensive, hand-aligned laboratory prototypes to be redesigned from low-cost components with tolerances suitable for mass manufacturing.

The optical imaging path is one such high-precision subcomponent. High storage density requires a lens with high numerical aperture operating near the diffraction limit over a wide field. A pixel-matched system additionally requires negligible field distortion and extremely tight focal-length tolerances to prevent magnification errors during media interchange. Further restrictions are imposed on allowable image

distortions because of media dimensional instability (e.g., shrinkage) and misalignment. Small errors in the mechanical registration of the holographic medium tend to produce displacement, rotation, and distortion of the holographic image without otherwise degrading its quality. Dynamic image alignment by microactuators leads to prohibitively large, expensive, and slow storage systems.

Although methods have been proposed for digitally restoring the fidelity of slightly misaligned images,^{3–5} realistic tolerance models indicate that image shifts of as many as several hundreds of micrometers might be encountered in the field. Algorithms based on Nyquist-rate oversampling of the irradiance pattern⁶ are prohibitive for megapixel data pages in terms of detector bandwidth, power, cost, and processing requirements.

An alternative approach, proposed by Burr,⁷ introduces a deliberate image magnification error into a system operating near the pixel-matched imaging condition, thus implementing sub-Nyquist rate oversampling. Such a configuration has the advantage of maintaining a low detector bandwidth while shifting the burden from preventing detector misalignment to measuring detector alignment. In the present paper we develop this approach further, proposing a practical system for alignment measurement together with an alternative resampling process.

The authors are with InPhase Technologies, Inc., 2000 Pike Road, Longmont, Colorado 80501. M. Ayres's e-mail address is markayres@inphase-tech.com.

Received 4 May 2005; revised 19 September 2005; accepted 25 October 2005; posted 3 November 2005 (Doc. ID 61814).

0003-6935/06/112459-06\$15.00/0

© 2006 Optical Society of America

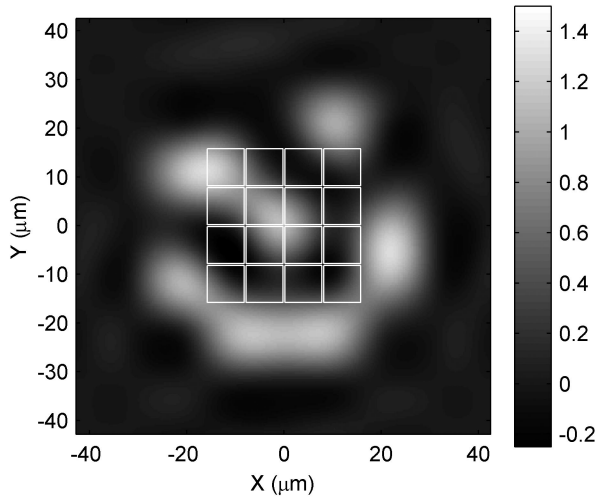


Fig. 1. Simulated data pixel image neighborhood (real part of complex amplitude).

2. Resampling Method

For holographic data storage it is advantageous to limit the spatial bandwidth of the object beam to only slightly higher than the Nyquist frequency of the data pattern. Typically an aperture in a Fourier plane is used to band limit the data beam (thereby also minimizing the size of the holograms in a Fourier-transform geometry). The data pattern may contain at most 1 cycle/2 data image pixels, so that the Nyquist frequency of the optical *field* of the object beam is minimally 1 sample/pixel. However, since the spectrum of the irradiance pattern is the autocorrelation of the spectrum of the optical *field*, the Nyquist frequency of the detectable signal is actually 2 linear samples/pixel minimum. Thus any method relying on less than 4 detector elements/data image pixel is operating in a sub-Nyquist regime where the Nyquist rate is defined with respect to the actual irradiance pattern impinging on the detector.

In the present method an estimate of the state of each data pixel is obtained by using only the detector elements in a 4×4 local window corresponding to the position of the data pixel image on the detector. Furthermore the estimation function is linear, excepting that a linearization exponent of 0.5 is applied to each detected intensity value in order to compensate for the nonlinear coherent addition of the data pixel images.⁸

A computer code was developed to simulate 5×5 neighborhoods of data pixel images impinging on the 4×4 detector element window, including diffraction effects, pixel fill factors, and coherent optical noise (Fig. 1). The code simulates the complex optical field impinging on the detector on a 256×256 sampled grid. The simulation was highly oversampled spatially with 32×32 samples representing each spatial light modulator (SLM) pixel. We effected optical propagation by composing an array representing the optical field of a single SLM pixel at the SLM plane and Fourier transforming the array to compute the field

at the polytopic aperture.⁹ The square aperture transmission function with width

$$D_p = 1.08 \frac{\lambda f}{\Delta_{\text{pix}}}, \quad (1)$$

where λ is the wavelength, f is the Fourier-transform lens focal length, and Δ_{pix} is the SLM pixel spacing, was applied multiplicatively. This limits the imaging resolution of the optical *field* to 1.08 times the Nyquist rate of the data pattern. The bandpassed optical field pattern was then inverse-Fourier transformed to generate the image field function for a single SLM pixel impinging on the detector. During the simulation, neighborhoods of SLM data patterns were built up in image space by superimposing shifted versions of this archetypical pixel image. (This architecture was adopted rather than Fourier propagating entire pixel neighborhoods so that pixel image functions incorporating aberrations and other higher-order effects could be easily imported into the simulation.) Finally the signal detected by each of the 16 detector elements was determined by taking the magnitude squared of the complex field function and summing it over the active area of each individual detector element.

A set of 16 linear coefficients is necessary to estimate the state of the central data pixel image from the 16 detected values. However, since the 4×4 detector window may have an arbitrary fractional alignment to the data pixel image, a single set of coefficients will not perform this task optimally. Therefore a different set of coefficients was generated for each possible fractional alignment. Results presented here utilize coefficients optimized for fractional alignments, δ_x, δ_y , in increments of 5% of the detector element spacing, resulting in a table with a size of $21 \times 21 = 441$ different 16-coefficient sets. The symmetry of the coefficients in both δ_x and δ_y allows for the simulation of only alignments $\delta_x, \delta_y = 0 \dots 0.5$ and generation of the other three quadrants of the table by symmetry.

Coefficient sets were derived over 2048 different binary states of the neighborhood for each fractional alignment case. Because it is impractical to simulate all 2^{25} possible states of the 5×5 SLM pixel neighborhood, a strategy was adopted whereby the inner 3×3 neighborhood (including the pixel of interest and its nearest neighbors) was swept through all 512 possible combinations 4 times, and the outer ring of pixels was assigned values randomly. This strategy was empirically demonstrated to possess good coefficient convergence properties.

The simulated detector values were used to determine resampling coefficients that satisfy the minimum mean-squared-error criterion; that is, the 16-element coefficient vector \mathbf{w} was selected so that

$$\hat{\mathbf{d}} = \mathbf{Iw}, \quad (2)$$

where

$$\|\hat{\mathbf{d}} - \mathbf{d}\|^2 = \sum_i (\hat{\mathbf{d}}_i - \mathbf{d}_i)^2$$

is minimized; \mathbf{I} is the 2048×16 matrix of linearized, simulated detector values; and \mathbf{d} and $\hat{\mathbf{d}}$ are 2048 element column vectors representing the binary states of the central SLM pixel in each neighborhood and the resampled estimates thereof, respectively. The solution, which may be given by¹⁰

$$\mathbf{w} = (\mathbf{I}^T)^{-1} \mathbf{I}^T \mathbf{d}, \quad (3)$$

was evaluated with an internal MATLAB function. Since the coefficients were selected to produce the minimum mean-squared-error estimate of the binary state of the central data pixel image (as opposed to, say, the irradiance value), the resampling process effectively removes much of the intersymbol interference. Finally a signal-to-noise ratio (SNR) metric

$$Q \equiv \frac{\mu_1 - \mu_0}{\sigma_1 + \sigma_0} \quad (4)$$

was defined to evaluate performance (where μ_1 and μ_0 are the means and σ_1 and σ_0 are the standard deviations of the resampled ones and zeros in $\hat{\mathbf{d}}$, respectively).

Of primary importance is the oversampling ratio itself. Figure 2 shows the effect of the oversampling ratio—defined as the data pixel image spacing divided by the detector element spacing—on the SNR for three local alignment cases. For these simulations, pixel areal fill factors for both the detector and the SLM were set to 90%, and coherent pseudorandom noise with a power of 1/20th of ON pixel power was added. The steep improvement for the poorly aligned case ($\delta_x = \delta_y = 0.5$, where the center of the data pixel image lands between the corners of four detector elements) as the oversampling ratio in-

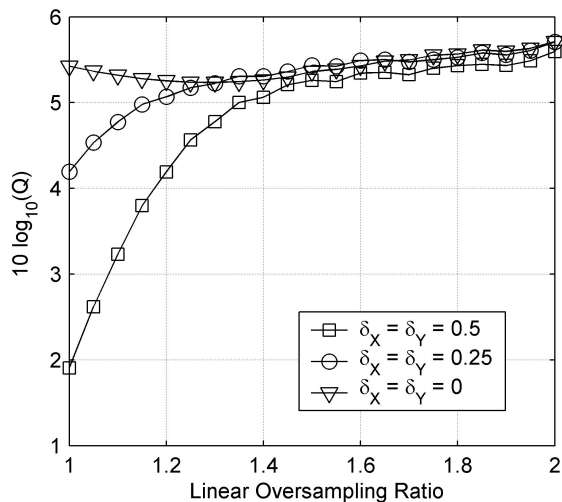


Fig. 2. Simulated effects of oversampling on the SNR for various local alignments.

creases from unity demonstrates the potential of this approach for relatively small ratios. Similarly the flatness of the curve near the Nyquist rate of the irradiance pattern (oversampling ratio ≈ 2) demonstrates the low marginal utility of increasing the ratio to that level.

The choice of an oversampling ratio hinges on a trade-off between performance, cost, and the complexity of the system. These factors will not be quantified here, but note that the total number of detector elements required goes up as the square of the oversampling ratio. Guided by these considerations (and available components), we constructed a demonstration unit by using a SLM with $12 \mu\text{m}$ pixels and a detector with $9 \mu\text{m}$ pixels yielding an oversampling ratio of 4/3.

This resampling approach differs substantially from the method in Ref. 7. In this former method an iterative decision feedback approach is used to remove both the coherent and the linear cross-talk contributions of the known data image pixel to its unknown neighbor. The process is repeated on an unknown neighbor of the now-known pixel. The method achieves its best performance when multiple passes are used (leftward, rightward, downward, and upward).

3. Alignment Measurement Method

The foregoing method requires the availability of sub-micrometer position information for each and every data pixel image. Alignment is derived from reserved blocks—small 8×8 SLM pixel datalike pseudorandom patterns that are distributed throughout the recorded data page on a grid at a spacing of 64 SLM pixels in both the x and the y directions (nominal areal overhead, 1.6%). The reserved blocks serve as fiducials for alignment measurement.

Reserved block position demodulation is accomplished through a covariance pattern-matching operation at a matrix of integer candidate positions within the detected image. The covariance matrix is calculated between the linearized detector values and a target pattern representing a resampled version of the interior 6×6 pixels of the binary reserved block pixel pattern. The actual SLM pixel patterns in the reserved blocks are selected by computer search so that the covariance between the central 6×6 pixels and any of the other 8 edge-bordering 6×6 pixel subblocks is exactly zero. This property ensures that the covariance values nearest the actual reserved block position reflect the fractional reserved block alignment rather than the noise created by the matching of random patterns. Synthesized patterns with other desired autocorrelation properties may be considered for further performance improvements,¹¹ although non-pattern-dependent noise seems to dominate accuracy for now.

The resampled target pattern is computed by choosing the largest square grid of detector elements that fit within the 6×6 reserved block center and then very simply integrating the binary pattern over the smaller detector pixel areas. No attempt was made to account for optical blur or pixel fill factors in

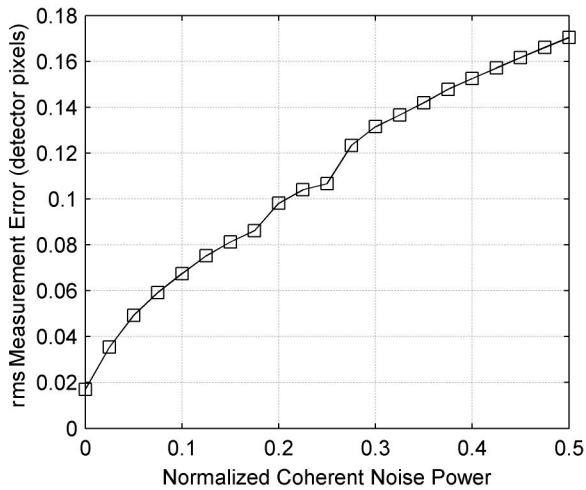


Fig. 3. Simulated reserved block demodulation measurement error versus coherent noise power (normalized to 1 = ON pixel).

this simplified resampling step. This facilitates variable oversampling ratio testing—the same reserved block patterns can be easily used at any ratio—but further performance gains may be possible by optimizing both the reserved block patterns and target pattern resampling for a specific ratio.

As stated in Section 1 it is desirable to allow for image displacement tolerances of as many as several hundred micrometers. Calculating a covariance matrix of this size would be computationally demanding. Furthermore much of the search area would contain uncontrolled data patterns that could randomly produce strong correlation peaks. For these reasons it is highly desirable to augment the technique with a preliminary coarse alignment measurement. Coarse x and y alignment for these experiments was determined by locating horizontal and vertical bar codes written in the page image borders. The accuracy of the coarse alignment, together with tolerances for image rotation and distortion, permitted the individual reserved blocks to be located to within ± 4 pixels, resulting in 9×9 element covariance matrices.

Once the covariance matrix is calculated, the maximum value is identified. The fractional part of the reserved block position is determined by linearly interpolating between the maximum and its immediate neighbors. Figure 3 is a plot of the simulated position demodulation error as a function of coherent noise. A typical reserved block pattern was demodulated at a diagonal series of 26 positions spanning ± 1.5 detector pixels, and the rms position measurement error was determined. The process was repeated for various coherent noise levels. The y intercept of $\sim 2\%$ error indicates the noise-free performance limit determined by suboptimal reserved block pattern or target selection.

The demodulation process is performed on all the reserved blocks within the data image, producing a grid of reserved block positions. Figure 4 shows the experimentally determined displacement from the nominal of a typical grid, illustrating a combination

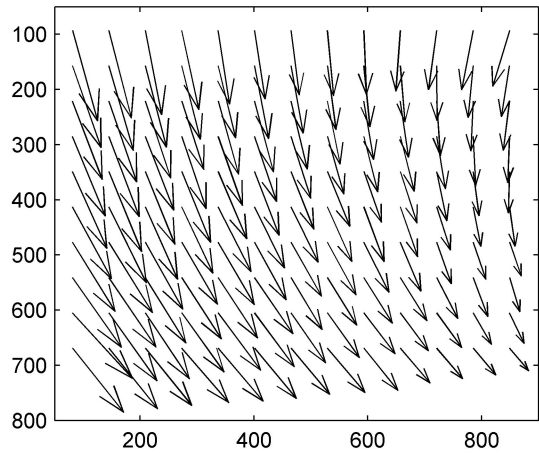


Fig. 4. Experimental data page reserved block displacement grid (arrow lengths, 64 times displacement).

of image shift, rotation, and demagnification. The grid is filtered to fill in any missing or anomalous values created by localized image defects. Finally the filtered grid is linearly interpolated to produce a map of the position of every data pixel image on the detector. The integer part of the position of the data pixel image is used to select the 4×4 detector window for resampling, and the fractional part (δ_x, δ_y) determines which coefficient set is used. Since the resampling process involves only the local alignment of individual data pixels, slowly varying distortions such as those illustrated in Fig. 4 are inconsequential.

Alignment mismeasurement sensitivity is a critical parameter for any processing algorithm based on alignment.⁵ Figure 5 shows the SNR of a single experimental holographic image resampled repeatedly while introducing a deliberate error in the x component of the alignment vector. The plot shows a negligible performance decrease for a 5% measurement error, indicating that the 5% resolution of the resampling coefficient table is adequate to the task.

Hardware implementation of the full algorithm presents some challenges. Because the alignment

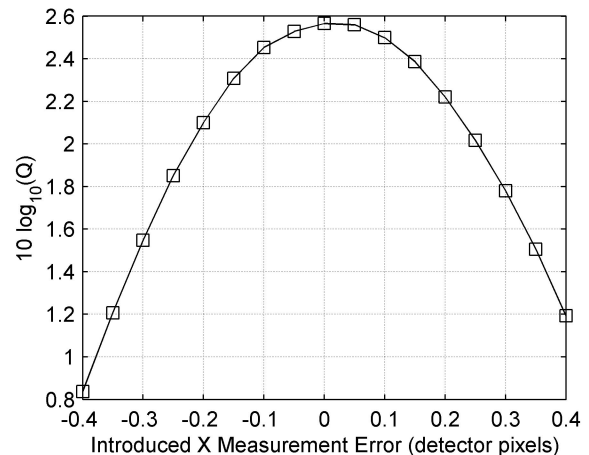


Fig. 5. Resampling sensitivity to alignment mismeasurement.

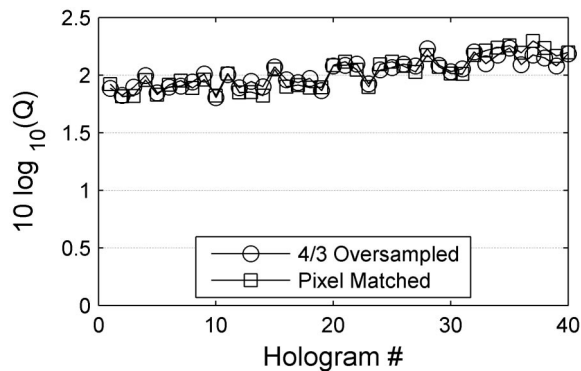


Fig. 6. Experimental SNR for angularly multiplexed holograms recovered with both pixel-matched and oversampled detectors.

information required by the resampling step is localized, there is some opportunity for pipelining the alignment measurement and resampling stages. A primary issue concerns the need to access the large coefficient lookup tables, possibly by several parallel resampling units. Possibilities for mitigating this problem include exploiting the coefficient symmetries on the fly to reduce table size and/or interpolating among coefficient values in a coarser table.

4. Experimental Results

The effectiveness of the method was validated experimentally by comparing holographic data pages recovered by using a pixel-matched detector with recoveries of the same holograms with the detector replaced by a 4/3 oversampled detector. Stacks of 100 angularly multiplexed holograms were recorded by using a 532 nm laser and a 720×720 , $12 \mu\text{m}$ pitch data page with a 92% pixel fill factor. The data were Fourier transformed and filtered with an aperture with a width 1.08 times Nyquist (roughly 0.95 mm square). The filtered Fourier-transformed data were then imaged into 1.5 mm thick InPhase Technologies Tapestry HDS3000 media. The resultant holograms were read out by using a 19 mW beam in a phase-conjugate configuration.² In nominal conditions the oversampled detector had a performance equal to that of the pixel-matched detector (see Fig. 6).

A slightly smaller data page (688×688 pixels) was used to test the tolerance of the recovery methods to detector gross misalignment. The smaller data page was chosen to give a border of 24 pixels ($\sim 0.22 \text{ mm}$) between the centered data page and the edge of the detector. When this data page was used, tolerance targets of $\pm 0.2 \text{ mm}$ displacement in the transverse directions, $\pm 0.4 \text{ mm}$ in focus, and $\pm 0.25^\circ$ of detector rotation were met without SNR penalties. The oversampled detector also achieved a higher SNR with weaker holograms than the pixel-matched detector. This result was obtained by varying the recording exposure time to control the strength of the holograms. Although the performance was equivalent with holograms of high diffraction efficiency, oversampled detection was more robust at lower diffraction efficiencies as shown in Fig. 7. Note that

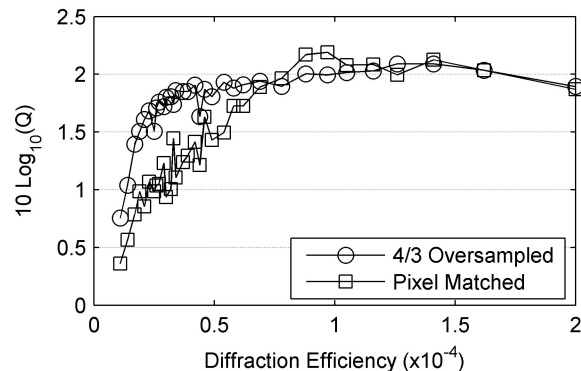


Fig. 7. Experimental SNR versus diffraction efficiency.

differing electrical characteristics and pixel fill factors between the detectors could have affected these results.

As a final demonstration of the effectiveness of the recovery method, stacks of holograms were stored in Tapestry HDS3000 by using a combination of angular and polytopic multiplexing.⁹ A total of 1200 720×720 data pages were stored in a 3×5 grid of angularly multiplexed stacks with 80 holograms/stack. The distance between the stacks was 4% larger than the linear polytopic aperture size (roughly a 1.0 mm stack pitch) resulting in a raw bit density of 26.8 Gbits/in.^2 (1 in. = 2.54 cm; limited by the small 4/3 oversampled detector size). The two detectors again performed equivalently.

5. Conclusions

A practicable method has been outlined for recovering stored data page images impinging on an unaligned, sub-Nyquist oversampled detector array. The method consists of a novel alignment measurement technique that uses covariance calculations to accurately locate pseudorandom fiducial marks and a linear resampling filter with coefficients that vary according to the local pixel alignment.

A laboratory demonstration was performed with an oversampling ratio of 4/3. Stacks of holograms were written and then read out with both a pixel-matched detector and an oversampled detector. Under nominal conditions the performance of oversampled detection was equal to that of pixel-matched detection. In increasingly marginal conditions (created by dropping the diffraction efficiency of the holograms), oversampled detection actually degraded more slowly than pixel-matched detection.

References

1. P. J. van Heerden, "Theory of optical information storage in solids," *Appl. Opt.* **2**, 393–400 (1963).
2. K. Curtis, W. L. Wilson, and L. Dhar, "High density holographic storage," in *Proceedings of the International Symposium on Optical Memory (ISOM, 2004)*.
3. P. Yoon, E. Hwang, B. Kang, J. Park, and G. Park, "Image compensation for sub-pixel misalignment in holographic data storage," *Proceedings of the International Symposium on Optical Memory (ISOM, 2004)*.
4. G. W. Burr and T. Weiss, "Compensation for pixel misregist-

- tration in volume holographic data storage," *Opt. Lett.* **26**, 542–544 (2001).
5. L. Menetrier and G. W. Burr, "Density implications of shift compensation postprocessing in holographic storage systems," *Appl. Opt.* **42**, 845–860 (2003).
 6. S. Redfield, "Tamarack optical head holographic storage," in *Holographic Data Storage*, H. J. Coufal, D. Psaltis, and G. Sincerbox, eds. (Springer-Verlag, 2000).
 7. G. W. Burr, "Holographic data storage with arbitrarily misaligned data pages," *Opt. Lett.* **27**, 542–544 (2002).
 8. V. Vadde and B. V. K. V. Kumar, "Channel modeling and estimation for intrapage equalization in pixel-matched volume holographic data storage," *Appl. Opt.* **38**, 4374–4386 (1999).
 9. K. Anderson and K. Curtis, "Polytopic multiplexing," *Opt. Lett.* **29**, 1402–1404 (2004).
 10. S. M. Kay, *Fundamentals of Statistical Signal Processing: Estimation Theory* (Prentice-Hall, 1993), Chap. 8.
 11. D. Calabro and J. K. Wolf, "On the synthesis of two-dimensional arrays with desirable correlation properties," *Inf. Control* **11**, 537–560 (1968).